



**HAL**  
open science

# Electromagnetic power and momentum in N-body hamiltonian approach to wave-particle dynamics in a periodic structure

Damien F G Minenna, Yves Elskens, Frédéric André, Fabrice Doveil

► **To cite this version:**

Damien F G Minenna, Yves Elskens, Frédéric André, Fabrice Doveil. Electromagnetic power and momentum in N-body hamiltonian approach to wave-particle dynamics in a periodic structure. EPL - Europhysics Letters, 2018, 122 (4), pp.44002. 10.1209/0295-5075/122/44002 . hal-01755085v2

**HAL Id: hal-01755085**

**<https://hal.science/hal-01755085v2>**

Submitted on 25 Sep 2019

**HAL** is a multi-disciplinary open access archive for the deposit and dissemination of scientific research documents, whether they are published or not. The documents may come from teaching and research institutions in France or abroad, or from public or private research centers.

L'archive ouverte pluridisciplinaire **HAL**, est destinée au dépôt et à la diffusion de documents scientifiques de niveau recherche, publiés ou non, émanant des établissements d'enseignement et de recherche français ou étrangers, des laboratoires publics ou privés.

## Electromagnetic power and momentum in $N$ -body hamiltonian approach to wave-particle dynamics in a periodic structure

Damien F. G. Minenna,<sup>1,2,3,\*</sup> Yves Elskens,<sup>2,†</sup> Frédéric André,<sup>3,‡</sup> and Fabrice Doveil<sup>2</sup>

<sup>1</sup>*Centre National d'Études Spatiales, 31401 Toulouse cedex 9, France*

<sup>2</sup>*Aix-Marseille University, UMR 7345 CNRS PIIM,*

*équipe turbulence plasma, case 322 campus Saint Jérôme,*

*av. esc. Normandie-Niemen, 13397 Marseille cedex 20, France*

<sup>3</sup>*Thales Electron Devices, rue Latécoère, 2, 78140 Vélizy, France*

(Dated: Received March 29, 2018; accepted in final form June 15, 2018; published online July 2, 2018)

(Dated September 25, 2019)

To model momentum exchange in nonlinear wave-particle interaction, as in amplification devices like traveling-wave tubes, we use an  $N$ -body self-consistent hamiltonian description based on Kuznetsov's discrete model, and we provide new formulations for the electromagnetic power and field momentum in media. This approach leads to fast and accurate numerical simulations in time domain and in one-dimensional space.

PACS numbers: 45.20.Jj (Lagrangian and hamiltonian mechanics), 52.40.Mj (Particle beam interaction in plasmas), 84.40.Fe (Microwave tubes)

Published as: Europhys. Lett. (EPL), **122** (2018) 44002 (7pp), doi: 10.1209/0295-5075/122/44002.

Note: This is the postprint version with minor corrections *\*in red\**.

The electromagnetic power and its density are major characteristics of amplifying devices and there is an increasing need to monitor them accurately in nonlinear regimes. While this power is generally computed using harmonic models, we undertake to compute it in position and time. To model the wave-particle interaction, we choose the particle description (a.k.a. discrete particle or  $N$ -body description), combined with a self-consistent hamiltonian [1–3], because nonlinear regimes are well addressed by considering the evolution of  $N$  nearly resonant charged particles interacting with the waves. Indeed, to predict turbulences and instabilities (due in particular to the chaotic dynamics of electrons) of the wave-particle system, the  $N$ -body description is the most intuitive approach. But it is also the most complex one in electrodynamics since the number of degrees of freedom for fields and particles involved is absolutely enormous. We propose a solution to this problem.

The interaction between an electron beam and electromagnetic waves is one of the most fundamental processes in the physics of hot and cold, natural, industrial and laboratory plasmas. This process is also at the heart of state-of-the-art wave amplifiers like vacuum electronic tubes (traveling-wave tubes (TWTs), klystrons, etc.), free electron lasers or particle accelerators. The key mechanism in this interaction is the exchange of momentum, as, *e.g.*, in the Landau effect [4, 5], when the phase velocity of the wave is close to the particles speed [6, 7]. Nowadays, the large power and broad band spectrum used in those electronic devices lead to critical instabilities and are difficult to simulate. For example, spurious frequencies are generated very far from the

drive frequency in the nonlinear regime because of drive-induced oscillations.

To follow particle motions and wave propagation in this interaction, we need better tools to study saturated nonlinear regimes, where electron motion perturbations become significant. Currently, two options are available to model such system, each with typical drawbacks. The first option is kinetic models in time domain such as particle-in-cell (PIC) algorithms based on Vlasov equations (like *e.g.* CST-PARTICLE and MAFIA) [8, 9]. But the resulting codes are extremely slow due to their large number of degrees of freedom. Therefore, they are not suitable for design activities and lead industry to rely on the second option : specialized algorithms in frequency domain. Those specialized models (like *e.g.* MVTRAD, BWIS and CHRISTINE) [10–12] are industrial standards because they are fast in their definition domains, but, based on our experiences, they are generally not rigorous to predict oscillation phenomena (including reflections and backward harmonic excitations) due to their nature. Besides, they are only partially consistent with Maxwell equations [13].

We propose a third option, using a many-body description to design a specialized model in time domain. By definition, this approach may involve a priori far more degrees of freedom than grid-based or spectral discretisations of the kinetic one. But a field decomposition provided by the Kuznetsov discrete model [14] allows us to drastically reduce the number of simulation parameters, for fields and particles as well.

The main purpose of this letter is to investigate the electromagnetic power distribution (eq. (28) below) in

the Kuznetsov discretization. Indeed, an important feature of traveling-wave tubes (TWTs) is the interaction efficiency (ratio between output power of the wave and electric power used by the device). Combining this model with the hamiltonian formalism [15] leads to a better respect of conservation properties in the model, including Poincaré-Cartan invariants [16], thanks to adapted symplectic algorithms [17, 18], allowing one to increase the numerical time step without incurring too much error on results. With the hamiltonian formalism, we compute the momentum balance (eq. (15)) in the wave-electrons interaction for a periodic structure, including the electromagnetic field momentum (eq. (22)) and its volume density (eq. (23)), from which we design a numerical integrator. Finally, simulations for a typical TWT will be run in one space dimension (1D), to be compared with a frequency algorithm to assess the accuracy of our time-domain approach.

This letter rests on ref. [15], which presents the construction of an electromagnetic hamiltonian, starting with the Kuznetsov discrete model [14, 19, 20]. Given the waveguide structure with period  $d$  along the  $z$ -axis, with period (cell) index  $n$ , this model provides an exact discretized decomposition of the radiofrequency (RF), divergence-free electromagnetic fields in the cell-based representation

$$\mathbf{E}(\mathbf{r}, t) = \sum_{s,n} \mathbf{V}_n^s(t) \mathbf{E}_{-n}^s(\mathbf{r}), \quad (1)$$

$$\mathbf{H}(\mathbf{r}, t) = i \sum_{s,n} \mathbf{l}_n^s(t) \mathbf{H}_{-n}^s(\mathbf{r}), \quad (2)$$

where  $s \in \mathbb{N}$  labels modes of propagation<sup>1</sup>. With the  $z$ -axis unit vector  $\mathbf{e}_z$ , time-independent basis fields  $\mathbf{E}_{-n}^s(\mathbf{r}) = \mathbf{E}_0^s(\mathbf{r} - nd\mathbf{e}_z)$ ,  $\mathbf{H}_{-n}^s(\mathbf{r}) = \mathbf{H}_0^s(\mathbf{r} - nd\mathbf{e}_z)$  are obtained ( $-n$  is a technical convention [15]) using Gel'fand transform (4), and depend only on the waveguide geometry. They do not obey orthogonality conditions in a simple cell; they decay (with oscillations) as  $|n - z/d| \rightarrow \infty$ , but do not plainly vanish for  $|n - z/d| > 1/2$ . Thus, total fields (1) and (2) at  $z$  essentially depend on nearby cells, allowing us to investigate finite structures. The  $i$  factor in (2) is a convenient choice, for which  $\mathbf{V}_n^s$  and  $\mathbf{l}_n^s$  are real-valued. In presence of electric sources, time-dependent coefficients  $\mathbf{V}_n^s$  and  $\mathbf{l}_n^s$  do not coincide, otherwise the system will violate Maxwell equations. Note that it is possible to use a linearised version of the discrete model [21, 22].

An advantage of this decomposition is that, for each mode of propagation (each “band”  $s$  in the dispersion diagram), there are  $2n_{\max}$  different time variables  $\mathbf{V}_n^s$  and

$\mathbf{l}_n^s$  (*viz.*  $n_{\max}$  degrees of freedom) for fields in a waveguide of  $n_{\max}$  periods. For example, space traveling-wave tubes are helical structure with  $n_{\max} \simeq 300$  periods. In comparison, finite difference techniques used in particle-in-cell codes necessitate millions of degrees of freedom to reach the same accuracy. Besides, this decomposition is exact regardless of the structure geometry provided it is periodic along the propagation direction.

Since terms  $\mathbf{V}_n^s$  and  $\mathbf{l}_n^s$  will be obtained from the hamiltonian dynamics, we must express the electromagnetic power using the discrete model. This is done below.

In the Kuznetsov discrete model, the  $n$ -based representation derives from a  $\beta$ -based representation<sup>2</sup> using Gel'fand transform [23]

$$G_\beta(\mathbf{r}, t) \stackrel{\text{def}}{=} \sum_{n \in \mathbb{Z}} G_n(\mathbf{r}, t) e^{in\beta d}, \quad (3)$$

with wavenumber  $\beta \in [-\pi/d, \pi/d]$ , and its inverse

$$G_n(\mathbf{r}, t) \stackrel{\text{def}}{=} (2\pi)^{-1} \int_{-\pi}^{\pi} G_\beta(\mathbf{r}, t) e^{-in\beta d} d(\beta d), \quad (4)$$

for an arbitrary function  $G$ . Those transforms allow to rewrite the electric field (1) as

$$\mathbf{E}(\mathbf{r}, t) = (2\pi)^{-1} \sum_s \int_{-\pi}^{\pi} \mathbf{V}_\beta^s(t) \mathbf{E}_\beta^s(\mathbf{r}) d(\beta d), \quad (5)$$

and similarly for the magnetic field with  $\mathbf{l}_\beta^s(t)$  and  $i\mathbf{H}_\beta^s(\mathbf{r})$ , where coefficients  $\mathbf{V}_\beta^s, \mathbf{l}_\beta^s$ , eigenfunctions  $\mathbf{E}_\beta^s, \mathbf{H}_\beta^s$  and frequency  $\Omega_\beta^s$  (used below) are  $\beta$ -based representations of respectively  $\mathbf{V}_n^s, \mathbf{l}_n^s, \mathbf{E}_n^s, \mathbf{H}_n^s$  and  $\Omega_n^s$  (used below). Explicit 1D projections of eigenfield  $\mathbf{E}_\beta^s$  are expressed by (31). These (propagating) modes are eigenvectors of the Helmholtz equation [14, 15, 19], with real eigenvalues  $\Omega_\beta^s$ ,

$$\text{rot } \mathbf{E}_\beta^s(\mathbf{r}) = -i\mu_0 \Omega_\beta^s \mathbf{H}_\beta^s(\mathbf{r}), \quad (6)$$

$$\text{rot } \mathbf{H}_\beta^s(\mathbf{r}) = i\epsilon_0 \Omega_\beta^s \mathbf{E}_\beta^s(\mathbf{r}), \quad (7)$$

for solenoidal eigenfields meeting the boundary conditions on the waveguide wall (e.g. perfect metal cylindrical or rectangular cavities) and the Floquet condition  $\mathbf{E}(\mathbf{r} + nd\mathbf{e}_z) = e^{-in\beta d} \mathbf{E}(\mathbf{r})$  in the  $z$  direction, so that the propagation constant  $\beta$  is the wavenumber associated with Bloch's theorem.

We normalize these eigenfields to

$$N_\beta^s \delta_{s'}^s = \int_{\mathcal{V}_0} \epsilon_0 \mathbf{E}_\beta^s \cdot \mathbf{E}_{\beta'}^{s'*} d^3\mathbf{r} = \int_{\mathcal{V}_0} \mu_0 \mathbf{H}_\beta^s \cdot \mathbf{H}_{\beta'}^{s'*} d^3\mathbf{r}, \quad (8)$$

<sup>1</sup> Label  $s$  is discrete-valued as it indexes eigenvalues  $\Omega_\beta^s$  (i.e. dispersion relations associated to field propagation) of the self-adjoint Helmholtz equation (6)-(7).

<sup>2</sup> In contrast with refs [15, 19], we let the phase per pitch,  $\beta d$ , range over  $[-\pi, \pi]$  instead of  $[0, 2\pi]$ , to enhance symmetry in calculations.

corresponding to the electric or magnetic energies stored in one period over the cell volume  $\mathcal{V}_0$ . For later convenience, this normalisation is chosen<sup>3</sup> equal to the eigenvalues  $\Omega_\beta^s$ . The Kronecker symbol  $\delta_{s'}$ , expressing orthogonality of modes  $s \neq s'$ , follows from the nondegeneracy of eigenvalues ( $\Omega_\beta^s \neq \Omega_\beta^{s'}$ ), which furthermore forces the integral  $\int_{\mathcal{V}_0} (\mathbf{E}_\beta^s \wedge \mathbf{H}_\beta^{s'*}) \cdot \mathbf{e}_z d^3\mathbf{r}$  to vanish.

Derivating (8) with respect to  $\beta$ , and using derivatives of Helmholtz eqs (6) and (7) and the derivative of the Floquet condition, yield the group velocity  $v_{g\beta}^s = \partial_\beta \Omega_\beta^s$  of the electromagnetic wave along the  $z$ -axis,

$$v_{g\beta}^s = \frac{d}{\Omega_\beta^s} \int_{\mathcal{S}} \Re(\mathbf{E}_\beta^s \wedge \mathbf{H}_\beta^{s'*}) \cdot \mathbf{e}_z d^2\mathbf{r}, \quad (9)$$

where  $\mathcal{S}$  is the transverse section of the waveguide.

Now, we recall the hamiltonian approach [15]. The Poynting energy  $H_{\text{em}} = \frac{1}{2} \int_{\mathcal{V}_Z} (\epsilon_0 |\mathbf{E}|^2 + \mu_0 |\mathbf{H}|^2) d^3\mathbf{r}$  over the system volume  $\mathcal{V}_Z$ , with normalisation (8) and the Parseval relation, yields the hamiltonian for radiative fields

$$H_{\text{em}} = \frac{1}{2} \sum_s \sum_{n_1, n_2} \left( \mathbf{V}_{n_1}^s \Omega_{n_1-n_2}^s \mathbf{V}_{n_2}^s + \mathbf{l}_{n_1}^s \Omega_{n_1-n_2}^s \mathbf{l}_{n_2}^s \right). \quad (10)$$

The normalisation (8) ensures that  $\mathbf{V}_n^s$  and  $\mathbf{l}_n^s$  are canonical variables<sup>4</sup>, satisfying the Poisson brackets  $\{\mathbf{V}_{n_1}^s, \mathbf{V}_{n_2}^{s'}\} = \{\mathbf{l}_{n_1}^s, \mathbf{l}_{n_2}^{s'}\} = 0$  and  $\{\mathbf{V}_{n_1}^s, \mathbf{l}_{n_2}^{s'}\} = \delta_{n_2}^{n_1} \delta_{s'}^s$ , with generalized coordinates  $\mathbf{l}_n^s$  and conjugate momenta  $\mathbf{V}_n^s$ .

The Fourier transform of  $\Omega_\beta^s$ , denoted  $\Omega_{n_1-n_2}^s$ , appears in (10) as the coupling coefficient between ‘‘RF oscillators’’ (or coupled cavities) at cells  $n_1$  and  $n_2$ . For coupled-cavity traveling-wave tubes, the actual dispersion relation is well described as a nearest-neighbour oscillator coupling, *viz.* with  $\Omega_n = 0$  for  $|n| \geq 2$  [19], whereas for helix traveling-wave tubes the coupling is longer-ranged (typically,  $|\Omega_n| > 0$  for  $|n| \leq 7$ ) [13, 24]. For the simulation below, we truncate coupling terms after 5 periods. This difference in the coupling coefficients reflects the properties of the underlying basis fields, which in turn reflect the actual geometry of the slow wave structure.

<sup>3</sup> As in [15], we choose  $N_\beta^s = \Omega_\beta^s$  which has the dimension of a pulsation, and then  $\mathbf{V}_n^s, \mathbf{l}_n^s$  are homogenous to the square root of an action. In [19], the normalisation has the dimension of an energy and  $\mathbf{V}_n^s$  and  $\mathbf{l}_n^s$  become dimensionless.

<sup>4</sup> Instead of these ‘‘cartesian’’ variables for oscillators, one can use the angle-action approach by considering  $\sqrt{2}\mathbf{C}_n^s(t) = \mathbf{V}_n^s(t) + i\mathbf{l}_n^s(t) \in \mathbb{C}$ , where canonical actions are  $\mathbf{C}_n^s \mathbf{C}_n^{s*}$ , with conjugate angles  $\theta_n^s = \text{Arg } \mathbf{C}_n^s$ . Then the electromagnetic hamiltonian (10) becomes

$$H_{\text{em}} = \sum_s \sum_{n_1, n_2} \mathbf{C}_{n_1}^s \mathbf{C}_{n_2}^{s*} \Omega_{n_1-n_2}^s. \quad (11)$$

The coupling with particles involves the longitudinal  $N$ -body dynamics [3, 15]. We consider a beam of  $N$  electrons with mass  $m$  and charge  $-|e|$ , labelled  $k$ , with positions  $z_k$  and canonical momenta  $p_k$ . The magnetic potential of the wave is rewritten with the cell-based representation (2) as  $\mathbf{A}(\mathbf{r}, t) = i \sum_{s,n} \mathbf{l}_n^s(t) \mathbf{A}_{-n}^s(\mathbf{r})$  (with Coulomb gauge  $\text{div } \mathbf{A} = 0$ ), where the basis magnetic potential  $\mathbf{A}_n^s$  is imaginary-valued<sup>5</sup> like  $\mathbf{H}_n^s$ . The electrons ballistic motion and their coupling with fields is given in one dimension by the relativistic hamiltonian

$$H_{\text{el}} = \sum_{k=1}^N mc^2 \left( \left[ 1 - \frac{\dot{z}_k^2}{c^2} \right]^{-1/2} - 1 \right) = \sum_{k=1}^N mc^2 (\gamma_k - 1), \quad (12)$$

with the Lorentz factor

$$\gamma_k = \left[ 1 + \left( p_k + |e| \sum_{s,n} i \mathbf{l}_n^s \mathbf{A}_{-n}^s(z_k) \right)^2 / (mc)^2 \right]^{1/2}. \quad (13)$$

The Coulomb interaction in the beam (possibly taking into account the waveguide wall boundary conditions) is incorporated through a scalar potential  $\phi$ . Then the Poynting energy splits into an RF contribution (10), and a space charge energy

$$H_{\text{sc}} = -\frac{1}{2} \sum_{k=1}^N \sum_{k' \neq k} |e| \phi(z_k - z_{k'}), \quad (14)$$

with the coulombian field  $E_{\text{sc},z} = -\partial_z \phi$  involving all charged particles of the system to interact with each other. The sum of (10), (12) and (14) is the total self-consistent hamiltonian for wave-particle dynamics along the  $z$ -axis.

In this formulation, the system total momentum (from Noether’s theorem) is the sum of electron (canonical) and field momenta

$$\mathbf{P}_{\text{wp},z} = \sum_{k=1}^N p_k + \sum_s \sum_{n_1, n_2} \mathbf{V}_{n_1}^s \mathbf{l}_{n_2}^s \mathbf{B}_{n_1-n_2}^s, \quad (15)$$

with the inverse Fourier transform of  $i\beta$

$$\mathbf{B}_n^s = -\mathbf{B}_{-n}^s = (2\pi)^{-1} \int_{-\pi}^{\pi} i\beta e^{-in\beta d} d(\beta d) \quad (16)$$

$$= \frac{(-1)^{n+1}}{nd} \quad \forall n \neq 0, \quad (17)$$

and  $\mathbf{B}_0^s = 0$ . The Legendre transform of the total hamiltonian is the lagrangian, for which Noether’s theorem

<sup>5</sup> In ref. [15], we write  $\mathbf{F}_n^s = -i\mathbf{A}_n^s$ . Note typos in ref. [15]: its equation (15) misses a minus sign in  $e^{-in\beta d}$ , and a  $c^2$  factor is missing in the second member of the second equation of its equation (26).

shows (15) to be conserved during the wave-electron momentum exchange. However, applying Noether's theorem is not trivial, as the waveguide geometry is not invariant under infinitesimal translations, but the lagrangian is invariant under  $z_k \mapsto z_k + \varepsilon, \mathbf{l}_\beta \mapsto e^{-i\beta\varepsilon}\mathbf{l}_\beta$ . Of course, the hamiltonian, being time-independent, is also the conserved total energy, though the energy does not split into a mere sum of individual, single-particle and single-mode contributions. Note that the wave-particle interaction is based on momentum exchange [3, 6], as implied by (15). The conservation of this momentum is essential to ensure that simulations are consistent.

Besides, we define the refractive kernel

$$\mathbf{K}_\beta^s = \frac{v_{g\beta}^s \Omega_\beta^s}{c^2} = \frac{\beta}{\mathbf{n}_{\phi\beta}^s \mathbf{n}_{g\beta}^s}, \quad (18)$$

with  $\mathbf{n}_{\phi\beta}^s = c/v_{\phi\beta}^s$  the phase refractive index,  $\mathbf{n}_{g\beta}^s = c/v_{g\beta}^s$  the group refractive index,  $v_{\phi\beta}^s = \Omega_\beta^s/\beta$  the phase velocity and  $v_{g\beta}^s$  the group velocity. The  $n$ -based representation of (18) from the group velocity  $v_{g\beta}^s = i \sum_n n d \Omega_n^s e^{in\beta d}$  is

$$\mathbf{K}_n^s = -\mathbf{K}_{-n}^s = (2\pi)^{-1} \mathfrak{R} \left[ \int_{-\pi}^{\pi} i \mathbf{K}_\beta^s e^{-in\beta d} d(\beta d) \right] \quad (19)$$

$$= c^{-2} d \sum_{n_2} (n_2 - n) \Omega_{n-n_2}^s \Omega_{n_2}^s. \quad (20)$$

This model is valid for any kind of waveform, but it simplifies in the monochromatic (a.k.a. continuous waveform, CW) regime, where the field is a sinusoidal wave with a single pulsation  $\omega = 2\pi F$ , of prime interest to applications. In this regime, phase and group velocities (and respective indices) can be considered as constant. This lead to the monochromatic approximation

$$\mathbf{B}_n^s \approx \mathbf{n}_\phi^s \mathbf{n}_g^s \mathbf{K}_n^s, \quad (21)$$

and the total field momentum (second term of (15)) is rewritten as

$$\mathbf{P}_{w,z}(t) \approx \sum_s \sum_{n_1, n_2} \mathbf{V}_{n_1}^s \mathbf{l}_{n_2}^s \mathbf{n}_\phi^s \mathbf{n}_g^s \mathbf{K}_{n_1-n_2}^s, \quad (22)$$

for sinusoidal fields. Note that, if we take the volume density of the Minkowski momentum in a dispersive waveguide<sup>6</sup>

$$\mathbf{g}_w(\mathbf{r}, t) = \mathbf{n}_\phi \mathbf{n}_g c^{-2} \mathbf{E}(\mathbf{r}, t) \wedge \mathbf{H}(\mathbf{r}, t) + \nabla u(\mathbf{r}, t), \quad (23)$$

where  $u$  is any function vanishing at boundaries, then the corresponding field momentum  $\mathbf{P}_{w,z}(t) = \int_{V_z} \mathbf{g}_w d^3\mathbf{r}$  is directly equal to (22), obtained from Noether's theorem.

The difference with the Abraham density of momentum  $c^{-2} \mathbf{E} \wedge \mathbf{H}$  is manifest [25].

The power of the RF electromagnetic wave is a key feature of vacuum electron devices. The fields representation (1)-(2) provides an expression for the power from the flux of the Poynting vector [26],  $\mathfrak{P}_z(z, t) = \int_S (\mathbf{E} \wedge \mathbf{H}) \cdot \mathbf{e}_z dS$ ,

$$\mathfrak{P}_z(z, t) = \sum_{s, s'} \sum_{n_1, n_2} \mathbf{V}_{n_1}^s(t) \mathbf{l}_{n_2}^{s'}(t) \mathfrak{K}_{n_1, n_2}^{s, s'}(z), \quad (24)$$

with

$$\mathfrak{K}_{n_1, n_2}^{s, s'}(z) = \int_S (\mathbf{E}_{-n_1}^s(\mathbf{r}) \wedge i \mathbf{H}_{-n_2}^{s'}(\mathbf{r})) \cdot \mathbf{e}_z dS. \quad (25)$$

The contribution of cell  $n$  to the electromagnetic field power propagation is the average flux (24) over the cell pitch

$$P_{z,n}(t) = \sum_{s, s'} \sum_{n_1, n_2} \mathbf{V}_{n_1}^s \mathbf{l}_{n_2}^{s'} \frac{1}{d} \int_{(n-\frac{1}{2})d}^{(n+\frac{1}{2})d} \mathfrak{K}_{n_1, n_2}^{s, s'}(z) dz. \quad (26)$$

These time-domain expressions are well suited for observing, for example, wave oscillations and transient reflections on the power, which would be impossible with frequency models. To obtain the contribution of each cell, we expand (26) by considering the  $z$ -dependence in  $\mathfrak{K}_{n_1, n_2}^{s, s'}$ . First, we note that, in  $\beta$ -representation, (26) involves two wave numbers  $\beta_1$  and  $\beta_2$  (from the Fourier transform on  $n_1$  and  $n_2$ ). In contrast with the second term in (15), we cannot impose  $\beta_1 = \beta_2$  by invoking destructive interference between different wavenumbers, because we consider a single cell  $(n-1/2)d < z < (n+1/2)d$ , not the full line  $-\infty < z < \infty$ .

To compute  $\mathfrak{K}_{n_1, n_2}^{s, s'}$ , we need the  $z$ -dependence of the basis fields  $\mathbf{E}_{n_1}^s, \mathbf{H}_{n_2}^{s'}$ , or equivalently of eigenfields  $\mathbf{E}_{\beta_1}^s, \mathbf{H}_{\beta_2}^{s'}$ . The main difficulty in (26) lies in the eigenmode cross-term (25). For  $\beta_1 = \beta_2$ , it relates directly with the group velocity (9). As a rule of thumb, because  $(\beta_1 - \beta_2)d$  is not very large in monochromatic regime, the simple approximation

$$\int_{(n-\frac{1}{2})d}^{(n+\frac{1}{2})d} \mathfrak{K}_{n_1, n_2}^{s, s'}(z) dz \approx c^2 \mathbf{K}_{n_1-n_2}^s \frac{1}{2} (\delta_{n_1}^n + \delta_{n_2}^n) \delta_s^{s'} \quad (27)$$

yields the estimated power in cell  $n$

$$P_{z,n}(t) \approx \frac{c^2}{d} \sum_s \sum_{n_2} \frac{1}{2} (\mathbf{V}_n^s \mathbf{l}_{n_2}^s - \mathbf{V}_{n_2}^s \mathbf{l}_n^s) \mathbf{K}_{n-n_2}^s, \quad (28)$$

which is time dependent, and where the geometric kernel  $\mathbf{K}_n^s$  depends on the dispersion relation  $\Omega_\beta^s$  (see eq. (20)) and not on transverse components of the field as (25).

<sup>6</sup> \*In the published version, it is wrongly defined as the electromagnetic field momentum density in a medium.\*

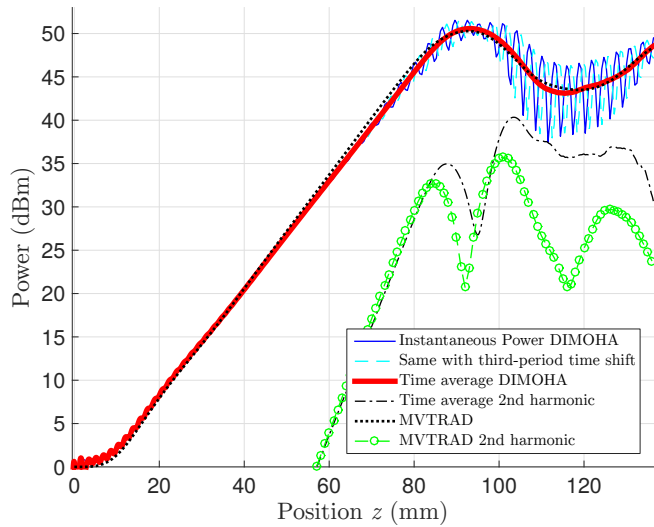


Figure 1. (Colour online) Spatial amplification of the electromagnetic power inside a model traveling-wave tube (no taper nor attenuations) for the fundamental mode ( $F = 12$  GHz) and its second harmonic from 1D time-domain simulation DIMOHA and frequency-domain algorithm MVTRAD. Continuous blue (resp. dashed cyan) curve : instantaneous power (28) at  $t_{\text{final}} = 6$  ns (resp. at  $t_{\text{final}} + 1/(3F)$ ). Thick red curve : power from (29), using for  $\tilde{E}_z$  the time Fourier transform of the electric field (1) (i.e. field envelope). Black dashed curve : its second harmonic. Black (resp. green) dots : fundamental (resp. second harmonic) power from MVTRAD.

To build an evolution algorithm from this formulation, we need the basis fields  $\mathbf{E}_n^s$  for (1). In this letter, we consider only one mode of propagation (we omit superscript  $s = 0$ ) and the thin beam approximation (axial 1D beam). This system is classically described by means of an equivalent circuit model [22, 27, 28] with a telegraph equation for the RF field, coupled with the beam. In the harmonic regime, the RF field evolves as  $E_z(\mathbf{r}, t) = \tilde{E}_z(\mathbf{r})e^{i\omega t}$  and generates locally the (time-averaged) power crossing section  $\mathcal{S}$  at abscissa  $z$ ,

$$\langle \mathfrak{P}_z \rangle = \frac{|\tilde{E}_z(r=0)|^2}{2\beta^2 Z_{c\beta}}, \quad (29)$$

with the wave impedance (a.k.a. circuit impedance)  $Z_{c\beta}$ . As the angular frequency  $\omega$  selects a single wavenumber  $\beta$ , the electric field on axis must also read  $\mathbf{V}_\beta(t)\mathbf{E}_{\beta,z}(z)$ , with eigenfield component  $\mathbf{E}_{\beta,z}(z)$  and amplitude  $\mathbf{V}_\beta(t) = \tilde{\mathbf{V}}_\beta e^{i\omega t}$ . And since the impedance  $Z_{c\beta}$  is defined regardless of any beam, (29) holds also without beam (“cold” regime of the device), with evolution equations reducing to  $\dot{\tilde{\mathbf{V}}}_\beta = i\tilde{\mathbf{I}}_\beta$ . Then the time-averaged flux of the Poynting vector (24) reduces to

$$\langle \mathfrak{P}_z \rangle = \frac{1}{2} \tilde{\mathbf{V}}_\beta^* i \tilde{\mathbf{I}}_\beta \frac{v_{g\beta} \Omega_\beta}{d}. \quad (30)$$

Finally, the longitudinal component of the electric field

on axis is proportional to  $e^{-i\beta z}$ . So the electric eigenfield shape function is<sup>7</sup>

$$\mathbf{E}_{z,\beta}(z) = e^{-i\beta z} \sqrt{\frac{v_{g\beta} \Omega_\beta}{d} \beta^2 Z_{c\beta}}. \quad (31)$$

The basis fields  $\mathbf{E}_n^s$  in 1D are given by the transform (4) of (31), and are similar to cardinal sine functions. In [15], we also have  $i\mathbf{A}_\beta^s = \mathbf{E}_\beta^s/\Omega_\beta^s$ , providing the magnetic potential eigenfield  $\mathbf{A}_n^s$ . Note that (31) involves only experimentally known values. To obtain the actual electric field in our time-domain modeling, for arbitrary waves and in presence of a beam, we only need to find coefficients  $\mathbf{V}_n(t)$ .

To benchmark our model, we run a one-dimensional numerical simulation with only the principal mode of propagation ( $s = 0$ ). The three hamiltonian terms (10), (12) and (14) generate simple evolution equations amenable to explicit discrete-time symplectic maps [16–18] for  $l_n$ ,  $\mathbf{V}_n$ ,  $z_k$  and  $p_k$ , providing a symplectic integrator. Physical model inputs are the dispersion relation  $\Omega_\beta$  and impedance  $Z_{c\beta}$ , which can be obtained experimentally or from a Helmholtz solver (given the structure geometry). For later comparisons, we take the dispersion relation used in [22] for a generic traveling-wave tube. These data yield the cell-based representation coefficients  $\Omega_n$  and  $\mathbf{K}_n$ , and field shape function  $\mathbf{E}_n(z)$ .

We simulate the beam as a line of  $N$  macro-electrons spaced from each other by  $\delta z_{\text{par}} = 1 \cdot 10^{-5}$  m, with identical initial speed  $\dot{z}_{\text{ini}} = 4.56 \cdot 10^7$  m/s and charge  $Q = 103\,270 e$  fixed by cathode potential and current values. The on-axis space-charge field in one dimension is obtained using Rowe’s approximation [20]. Fields are discretized on a grid with mesh  $\delta z_{\text{field}}$ . Time-sinusoidal waves are excited at the first cell by adding a forcing term  $2\pi F U \sin(2\pi F t)$  to  $\dot{\mathbf{V}}_1$  in the integrator, with frequency  $F = 12$  GHz, and appropriate amplitude  $U$  to ensure<sup>8</sup>  $\mathfrak{P}_z(z=0) = 1$  mW. Note that generation of second harmonic occurs in TWTs. To represent the waveguide beginning and end on the  $z$ -axis, we broke conservation properties by appending long attenuators on either side to damp  $\mathbf{V}_{n'}(n' < 0$  or  $n' > n_{\text{end}})$  at a small rate in space.

The comparison is performed versus algorithm MVTRAD [10] (property of Thales Electron Devices), an industrial code in frequency domain (or so-called envelope model), well-used and robust to simulate industrial

<sup>7</sup> Note a difference by a  $\sqrt{2}$  factor in [20] due to missing the  $1/2$  prefactor in the harmonic regime (the usual factor for average power using peak amplitudes) in front of (30). Numerical comparisons with experimental data validate our relation without the  $\sqrt{2}$  factor.

<sup>8</sup> To characterize the gain, in Fig. 1 we plot the power logarithmic ratio  $10 \log_{10}(\mathfrak{P}_z(z)/\mathfrak{P}_z(0))$ , which defines the dBm scale in electronics.

traveling-wave tubes (TWTs). It was specifically designed to investigate saturation regimes (including first trapping oscillations in nonlinear regimes) for sinusoidal waves, thus we operate it in a working regime where it has been properly validated. But because of its conception from the frequency domain, MVTRAD cannot simulate oscillation with drive nor predict reflections and spurious oscillation phenomena (a main cause of instability in TWTs). Time-domain models will not suffer from those limitations.

Since the aim of this paper is mostly to present theoretical tools for wave-particle simulations rather than to design a complete algorithm for scientific and industrial purposes, we focus on a single numerical comparison. Benchmarking with simulations and experimental data over wide ranges will be done in a separate work, with our algorithm modified to account for current TWT defects (such as losses and attenuations or tapering): in the present letter, we focus on the fundamental physical process of momentum exchange.

Fig. 1 presents a comparison between the electromagnetic power computed with our approach (DIMOHA for HAmiltonian DIcrete MOdel) and MVTRAD. Initial parameters (like cathode current and potential, coupling impedances, phase velocity, tube length) are set to ensure that the amplification leads the power to saturation before the end of the tube, and space charge effects are taken into account. Our instantaneous power (28) at a time  $t_{\text{final}} = 6$  ns is plotted (continuous thin blue curve). The cyan curve is also the instantaneous power (28), but at the time  $t_{\text{final}} + 1/(3F)$ , and demonstrates that (28) follows the wave propagation with time. The thick red curve is the power from (29), where we take the time Fourier transform over one time-period of the electric field (1), and the black dashed curve is its second harmonic.

Fig. 2 shows the electron velocity ratio  $\dot{z}_k(t_{\text{max}})/\dot{z}_{\text{ini}}$  and exhibits nonlinear effects (trapping) occurring approximately after  $z = 60$  mm (some particles crossed the separatrix centered on  $v_{\text{ph}}$  [3, 29]). The power saturation occurs at  $z = 90$  mm, when trapped particles start to regain momentum at the wave expense in agreement with the conservation law (15).

Agreement, in Fig. 1, between the frequency aspect of the discrete model, *viz.* time-averaged power (29), and MVTRAD (black dots) is excellent for the fundamental mode (actually, the discrepancy hardly catches the eye). Oscillations for the instantaneous time power (28) occur in nonlinear regime. Since electrons are bunched with a period near  $1/F$  (visible in Fig. 2), large oscillations of instantaneous time power (28) occur in nonlinear regime, when the modulation of electrons velocities becomes important. Time average of instantaneous power (28) over the wave period is not shown because it is indistinguishable from the power (29) (red curve) from the field envelope. Small variations between our approach

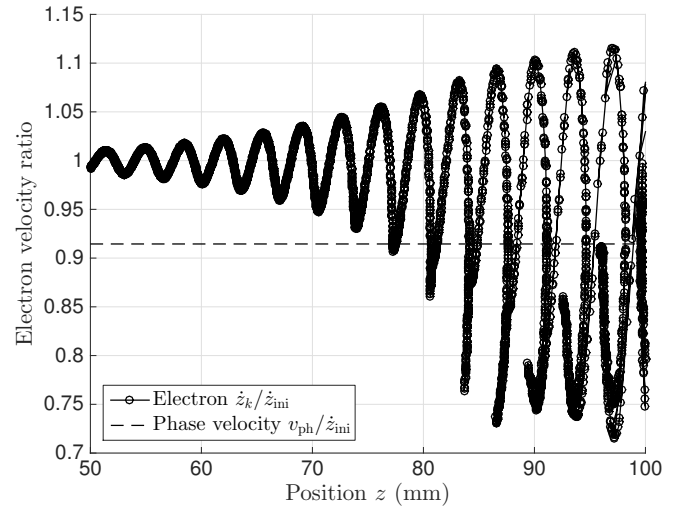


Figure 2. Ratio of the speed of electron  $\dot{z}_k(t_{\text{max}})/\dot{z}_{\text{ini}}$  for the simulation of Fig. 1, at  $t_{\text{max}} = 6$  ns. The beam at  $z = 0$  is mono-kinetic and starts slowly to oscillate with a period near  $1/F$ . Dashed line : phase velocity  $v_{\text{ph}}/\dot{z}_{\text{ini}}$ .

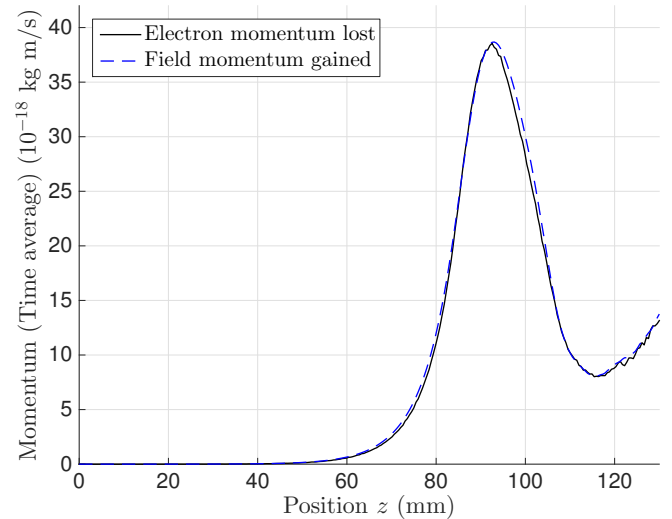


Figure 3. (Colour online) Wave-particle momentum conservation per cell for the simulation of Fig. 1. Continuous black curve : time average over one wave period  $1/F$  of canonical momentum lost (32). Dashed blue curve : time average of field momentum (33).

and MVTRAD (green circles), such as a bias in saturation power, appear for the power's second harmonic. But second harmonic experimental measurements are difficult to perform accurately. Both our model and MVTRAD remain within experimental uncertainty.

To assess momentum conservation (15) by our algorithm, we compare, in the cell representation, the canon-

ical momentum<sup>9</sup>

$$-P_{p,n} = - \sum_{k'(n)} \left( p_{k'}(t) - p_{ini} \right), \quad (32)$$

lost by particles  $k'(n) : |z_{k'} - nd| < d/2$  inside the cell  $n$  and the estimated wave momentum in cell  $n$

$$P_{w,n} \approx \sum_{n_2} \frac{1}{2} (V_{n_1} I_{n_2} - V_{n_2} I_{n_1}) n_{\phi} n_g K_{n-n_2}, \quad (33)$$

for the dominant propagating mode. Part of the calculation is the same as for the power per cell, using approximation (27). Note that application of Noether's theorem requires a translation invariant system. Since the system we simulate is open, we can expect small discrepancies. Momentum provided by the field excitation at cell 1 is neglected since the amplification (up to 50 dBm) is large enough. Fig. 3 displays the time average over one wave period  $1/F$  of canonical<sup>10</sup> (32) and field (33) momenta<sup>11</sup>. The agreement is excellent. An almost identical result is obtained when replacing  $n_{\phi} n_g K_n$  by  $B_n$  in (33) (indistinguishable on Fig. 3).

In this work, starting from a total hamiltonian describing the coupling between an electron beam and the radiative fields propagating in a periodic waveguide, and using a field discretization, we constructed the conserved momentum of the system, and the instantaneous and time-averaged electromagnetic power. We built a time-domain algorithm which is much faster than industrial PIC codes (running in the scale of seconds) and as accurate as a frequency-domain algorithm in tested regimes.

But this approach goes further than frequency models, as it enables to address situations in nonlinear regimes with trapped and chaotic particles interacting with fields, which is of interest to a broader community of physicists and engineers [30]. While the  $N$ -body description was, for a long time, deemed impossible for microscopic plasma physics (until recently [31]), this letter proves that this description can be useful, even for industrial devices like TWTs. Moreover, the total hamiltonian we propose is intuitive and easy to understand with our approach.

Oscillations, reflections and multitone operation are currently investigated in addition with the electromagnetic field momentum in media. We are also working on two- and three-dimensional versions of the model to provide a complete electron velocity and position distribution (e.g. to improve the conception of collectors at the

end). To validate our approach, comparison with experimental TWTs will be performed (see [24] for preliminary results), after taking into account losses and tube defects.

The authors gratefully acknowledge fruitful comments from D. Escande and constructive questions from anonymous reviewers.

\* Electronic address: damien.minenna@univ-amu.fr

† Electronic address: yves.elskens@univ-amu.fr

‡ Electronic address: frederic.andre@thalesgroup.com

- [1] MYNICK H. E. KAUFMAN A. N., *Phys. Fl.*, **21** (1978) 653-663.
- [2] TENNYSON J. L., MEISS J. D. MORRISON P. J., *Physica D*, **71** (1994) 1-17.
- [3] ELSKENS Y. ESCANDE D. F., *Microscopic dynamics of plasmas and chaos* (IoP publishing, Bristol) (2003).
- [4] LANDAU L., *J. Phys. USSR*, **10** (1946) 25-34.
- [5] O'NEIL T. M., WINFREY J. H. MALMBERG J. H., *Phys. Fl.*, **14** (1971) 1204-1212.
- [6] DOVEIL F., ESCANDE D. F. MACOR A., *Phys. Rev. Lett.*, **94** (2005) 085003 (4 pp.).
- [7] DOVEIL F., ELSKENS Y. MINENNA D. F. G., *Wave-Particle Interaction studied in a Traveling Wave Tube, invited talk at ICPP 2018, Vancouver, 2018*.
- [8] SAFI D., BIRTEL P., MEYNE S. JACOB A. F., *IEEE Trans. Electron Devices*, **65** (2018) 2257-2263.
- [9] WEILAND T. *et al.*, *AIP Conf. Proc.*, **391** (1997) 65-70.
- [10] WALLER P., *Modélisation numérique de l'interaction et diagnostic expérimental du faisceau d'électrons dans un tube à ondes progressives spatiales*, PhD thesis, Université Paris 7, (1999).
- [11] LI B., YANG Z. H., LI J. Q., ZHU X. F., HUANG T., HU Q., HU Y. L., XU L., MA J. J., LIAO L. XIAO L., *IEEE Trans. Electron Devices*, **56** (2009) 919-927.
- [12] ANTONSEN T. M. JR LEVUSH B., CHRISTINE : *a multi-frequency parametric simulation code for traveling wave tube amplifiers* (Washington DC) (1997).
- [13] THÉVENY S., ANDRÉ F. ELSKENS Y., *On frequency and time domain models of traveling wave tubes*, <https://hal.archives-ouvertes.fr/hal-01340471> (2016).
- [14] KUZNETSOV S. P., *Sov. J. Commun. Technol. Electron.*, **25** (1980) 419-421.
- [15] ANDRÉ F., BERNARDI P., RYSKIN N. M., DOVEIL F. ELSKENS Y., *EPL*, **103** (2013) 28004 (5 pp).
- [16] ARNOLD V. I., *Mathematical Methods of Classical Mechanics* (Springer-Verlag) (1989).
- [17] HAIRER E., LUBICH CH. WANNER G., *Acta Num.*, **12** (2003) 399-450.
- [18] HAIRER E., LUBICH CH. WANNER G., *Geometric numerical integration : Structure-preserving algorithms for ordinary differential equations* (Springer, New York) (2010).
- [19] RYSKIN N. M., TITOV V. N. YAKOVLEV A. V., *IEEE Trans. Electron Devices*, **56** (2009) 928-934.
- [20] BERNARDI P., ANDRÉ F., DAVID J-F., LE CLAIR A. DOVEIL F., *IEEE Trans. Electron Devices*, **58** (2011) 1761-1767.
- [21] TERYTYUK A. G. RYSKIN N. M., Private communication.

<sup>9</sup> \*Note a typo in the published version:  $p'_k$  should read  $p_{k'}$ .\*

<sup>10</sup> \*In the published version: mechanical should read canonical.\*

<sup>11</sup> The scale  $10^{-18}$  N-s results from the tiny electron mass and from field momentum being proportional to  $c^{-2}$  (see (20)).

- [22] MINENNA D. F. G., THERENTYUK A. G., ANDRÉ F., ELSKENS Y. RYSKIN N. M., (2017) arxiv:1711.04510, \*now published as *Phys. Scr.*, **94** (2019) 055601, doi: 10.1088/1402-4896/ab060e.\*.
- [23] GEL'FAND I. M., *Dokl. Akad. Nauk SSSR*, **73** (1950) 1117-1120.
- [24] MINENNA D. F. G., ELSKENS Y. ANDRÉ F., *Electron-wave momentum exchange and time domain simulations applied to traveling wave tubes* (18th IEEE IVEC, London) (2017).
- [25] PFEIFER R. N. C., NIEMINEN T. A., HECKENBERG N. R. RUBINSZTEIN-DUNLOP H., *Rev. Mod. Phys.*, **79** (2007) 1197-1216.
- [26] JACKSON J. D., *Classical Electrodynamics*, 3<sup>rd</sup> edition (Wiley, New York) (1999).
- [27] PIERCE J. R., *Traveling wave tubes* (Van Nostrand, New York) (1950).
- [28] ANDRÉ F. AÏSSI A., *IEEE Trans. Electron Devices*, **57** (2010) 1687-1695.
- [29] CUTLER C. C., *Bell Labs Tech. J.*, **35** (1956) 841-876.
- [30] DOVEIL F. MACOR A., *Phys. Plasmas*, **13** (2006) 055704 (5 pp.).
- [31] ESCANDE D. F., BÉNISTI D., ELSKENS Y., ZARZOSO D. AND DOVEIL F., *Basic microscopic plasma physics from N-body mechanics: A tribute to Pierre-Simon de Laplace*, <https://hal.archives-ouvertes.fr/hal-01802414> (2018), \*now published as *Rev. Mod. Plasma Phys.*, **2** (2018) 9 (68 pp.)\*.